An Active Pulse Transmission Line Simulating Nerve Axon*

J. NAGUMO†, MEMBER, IRE, S. ARIMOTO†, AND S. YOSHIZAWA†

Summary—**To electronically simulate an animal nerve axon, the authors made an active pulse transmission line using tunnel diodes. The equation of propagation for this line is the same as that for a simplified model of nerve membrane treated elsewhere. This line shapes the signal waveform during transmission, that is, there being a specific pulse-like waveform peculiar to this line, smaller signals are amplified, larger ones are attenuated, narrower ones are widened and those which are wider are shrunk, all approaching the above-mentioned specific waveform. In addition, this line has a certain threshold value in respect to the signal height, and signals smaller than the threshold or noise are eliminated in the course of transmission. Because of the above-mentioned shaping action and the existence of a threshold, this line makes possible highly reliable pulse transmission, and will be useful for various kinds of information-processing systems.**

I. Introduction

IN THE CASE of conventional pulse transmission lines, provided they are of great length, signals suffer attenuation and distortion as they travel down the line, whereas an electric pulse signal which is transmitted along an animal nerve axon suffers neither attenuation nor distortion, regardless of the distance covered. A pulse transmission line with such qualities will be useful for pulse transmission in communication systems, data processing systems, electronic computers, etc.

It is our purpose to realize such a pulse transmission line by simulating the animal nerve axon.

II. Excitation of Nerve Axon

A great deal of research on the electro-physiology of the nerve axon has already been made,[1] the most important being that of Hodgkin and Huxley.[2] They have made a quantitative study of the excitation of a nerve axon and the propagation of the excitation, and have derived the Hodgkin-Huxley equations (H-H equations) which describe the phenomena.

In the case of a "space clamp," that is, in a case where the excitation of a nerve axon is spacially uniform, the H-H equations describing the excitation of the nerve axon are as follows (see Appendix):

$$\begin{cases} I = C_0 \dfrac{dV}{dt} + \bar{g}_{Na} m^3 h (V - V_{Na}) + \bar{g}_K n^4 (V - V_K) \\ \qquad + \bar{g}_L (V - V_L), \\ \dfrac{dm}{dt} + \{\alpha_m(V) + \beta_m(V)\} m = \alpha_m(V), \\ \dfrac{dh}{dt} + \{\alpha_h(V) + \beta_h(V)\} h = \alpha_h(V), \\ \dfrac{dn}{dt} + \{\alpha_n(V) + \beta_n(V)\} n = \alpha_n(V), \end{cases} \tag{1}$$

$$\alpha_m(V) = 0.1(V + 25)\left[\exp\left(\frac{V + 25}{10}\right) - 1\right]^{-1},$$

$$\beta_m(V) = 4 \exp\left(\frac{V}{18}\right),$$

$$\alpha_h(V) = 0.07 \exp\left(\frac{V}{20}\right),$$

$$\beta_h(V) = \left[\exp\left(\frac{V + 30}{10}\right) + 1\right]^{-1},$$

$$\alpha_n(V) = 0.01(V + 10)\left[\exp\left(\frac{V + 10}{10}\right) - 1\right]^{-1},$$

$$\beta_n(V) = 0.125 \exp\left(\frac{V}{80}\right),$$

where

I = the membrane current density (μa/cm^2) [inward current positive],
V = the membrane voltage (mV) [difference from resting potential, depolarization negative],
m = the sodium activation (dimensionless) [varying between 0 and 1],
h = the sodium inactivation (dimensionless) [varying between 0 and 1],
n = the potassium activation (dimensionless) [varying between 0 and 1],
t = time (msec),
C_0 = the membrane capacitance (μf/cm^2),
$\bar{g}_{Na} = 120$, $\bar{g}_K = 36$, $\bar{g}_L = 0.3$ (m$\mho$/cm^2),
$V_{Na} = -115$, $V_K = 12$, $V_L = -10.5989$ (mV).

* Received April 26, 1962; revised manuscript received July 9, 1962.

† Dept. of Applied Physics, Faculty of Engineering, University of Tokyo, Tokyo, Japan.

[1] Readers unfamiliar with the electro-physiology of the nerve axon may wish to refer to J. W. Moore, "Electronic control of some active bioelectric membranes," PROC. IRE, vol. 47, pp. 1869–1880; November, 1959.

[2] A. L. Hodgkin and A. F. Huxley, "A quantitative description of membrane current and its application to conduction and excitation in nerve," *J. Physiol.*, vol. 117, pp. 500–544; August, 1952.

Several investigations of the H-H equations by the use of analog computers[3,4] and digital computers[5-8] have appeared in recent literature. Nevertheless, it is still difficult to make an electronic simulator of the H-H equations on account of their complexities.

III. The BVP Model

Recently, FitzHugh ingeniously simplified the H-H equations in case of a "space clamp," making use of an analog computer, and proposed the following BVP model (Bonhoeffer-van der Pol model).[9]

$$\begin{cases} J = \dfrac{1}{c}\dfrac{du}{dt} - w - \left(u - \dfrac{u^3}{3}\right), \\ c\dfrac{dw}{dt} + bw = a - u, \end{cases} \tag{2}$$

where a, b and c are constants satisfying the relations

$$1 > b > 0, \quad c^2 > b, \quad 1 > a > 1 - \tfrac{2}{3}b. \tag{3}$$

The variables u, w and J in the BVP model (2) correspond to the pair of variables (V, m), the pair of variables (h, n) and I in (1), respectively.

Fig. 1(a) shows the trajectories on the (u, w)-plane of the BVP model (2) in the case where $J=0$, while Fig. 1(b) shows the trajectories on the (u^*, w^*)-plane of (1) in the case where $I=0$. Here,

$$u^* = V - 36m, \qquad w^* = \tfrac{1}{2}(n - h). \tag{4}$$

Comparing Fig. 1(a) to Fig. 1(b), it is observed that there is fairly good correspondence between the H-H equations and the BVP model. We shall therefore try to simulate (2) instead of (1).

IV. An Electronic Simulation of the BVP Model

Let us consider the two-terminal circuit of Fig. 2, where TD is a tunnel diode.[10] From Kirchhoff's law

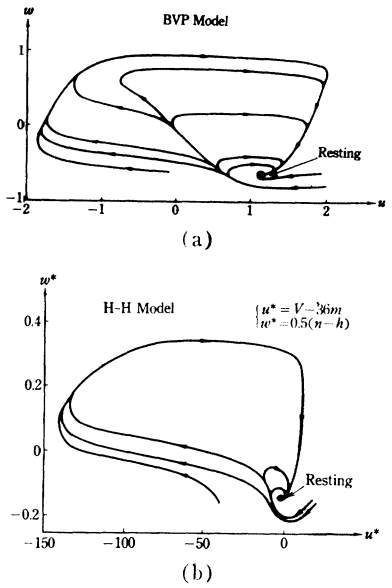

Fig. 1—The qualitative similarity of (a) and (b) suggests that the BVP model can be considered as belonging to the same class of excitable systems as the Hodgkin-Huxley model. (Reproduced from FitzHugh,[9] courtesy of the author.)

$$\begin{cases} j = C\dfrac{dv}{d\tau} - i - f(e), \\ L\dfrac{di}{d\tau} + Ri = -v = e - E_0, \end{cases} \tag{5}$$

where $f(e)$ is a function, as shown in Fig. 3, which represents the voltage vs current characteristic of the tunnel diode. For simplicity, we assume

$$f(e) = i_0 - \frac{1}{\rho}\left\{(e - e_0) - \frac{(e - e_0)^3}{3K^2}\right\} \quad (\rho > 0,\ K > 0), \tag{6}$$

where

$$i_0 = f(e_0).$$

By the introduction of new variables

$$t = \frac{\tau}{\sqrt{LC}}, \quad u = \frac{v + (e_0 - E_0)}{K}, \quad w = \frac{\rho}{K}(i + i_0),$$

$$J = \frac{\rho}{K}j, \quad a = \frac{Ri_0 + (e_0 - E_0)}{K}, \quad b = \frac{R}{\rho},$$

$$c = \frac{1}{\rho}\sqrt{\frac{L}{C}},$$

it is seen that (5) is reduced to (2).

Next, we shall examine the conditions in (3) for the constants a, b and c.

The first condition: $1 > b > 0$ is equivalent to

$$\rho > R. \tag{7}$$

The second condition: $c^2 > b$ is equivalent to

$$\frac{L}{R} > \rho C. \tag{8}$$

[3] G. A. Bekey and B. Paxon, "Analog Simulation of Nerve Excitation," presented at the 2nd National Simulation Conference, Houston, Texas; April, 1957.
[4] R. FitzHugh, "Thresholds and plateaus in the Hodgkin-Huxley nerve equations," *J. Gen. Physiol.*, vol. 43, pp. 867–896; May, 1960.
[5] K. S. Cole, H. A. Antosiewicz, and P. Rabinowitz, "Automatic computation of nerve excitation," *J. Soc. Indust. Appl. Math.*, vol. 3, pp. 153–172; September, 1955.
[6] ——"Automatic computation of nerve excitation, correction," *J. Soc. Indust. Appl. Math.*, vol. 6, pp. 196–197; June, 1958.
[7] R. FitzHugh and H. A. Antosiewicz, "Automatic computation of nerve excitation, detailed corrections and additions," *J. Soc. Indust. Appl. Math.*, vol. 7, pp. 447–458; December, 1959.
[8] R. FitzHugh, "Computation of impulse initiation and saltatory condition in a myelinated nerve fiber," *Biophysical J.*, vol. 2, pp. 11–21; January, 1962.
[9] R. FitzHugh, "Impulses and physiological states in theoretical models of nerve membrane," *Biophysical J.*, vol. 1, pp. 445–466; July, 1961.
[10] J. Nagumo, *et al.*, "An Active Line Using Esaki Diodes," Inst. Elec. Commun. Engrs. Japan, Professional Group on Nonlinear Circuit Theory, Rept.; February 7, 1961 (in Japanese).

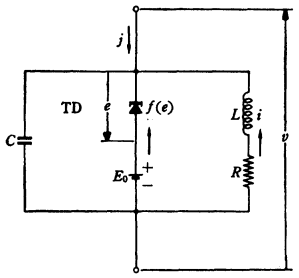

Fig. 2—An electronic simulator of the BVP model.

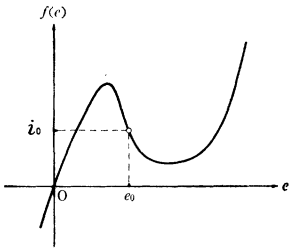

Fig. 3—The voltage-current characteristic of the tunnel diode.

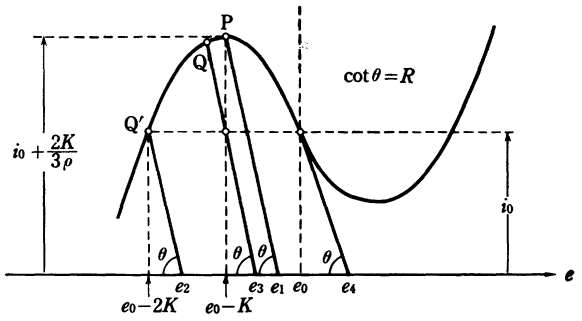

Fig. 4—When bias voltage E_0 is set between e_1 and e_2, the circuit shown in Fig. 2 is monostable. Whereas, if $E_0=e_4$, the circuit oscillates spontaneously.

The last condition: $1>a>1-\frac{2}{3}b$ is equivalent to

$$Ri_0 + (e_0 - K) < E_0 < R\left(i_0 + \frac{2K}{3\rho}\right) + (e_0 - K), \quad (9)$$

or

$$e_3 < E_0 < e_1, \quad (10)$$

in Fig. 4.

The conditions in (7), (8) and (10) imply that in the case of the "current clamp," $j=0$, the circuit shown in Fig. 2 is nothing but the well-known monostable circuit of the tunnel diode. In particular, the condition in (8) means that the circuit oscillates spontaneously if the bias voltage is set at e_4 in Fig. 4. In fact, if $E_0=e_4$, then $a=0$, and in the case of $j=0$, (2) becomes as follows:

$$\frac{d^2u}{dt^2} - c\left\{\left(1 - \frac{b}{c^2}\right) - u^2\right\}\frac{du}{dt} + \left\{(1-b)u + \frac{b}{3}u^3\right\} = 0. \quad (11)$$

Since $c^2>b$, $1>b>0$, $c>0$, this differential equation belongs to the Liénard type[11] which represents self-oscillations.

Therefore it is concluded that the BVP model can be simulated by the monostable circuit shown in Fig. 2. However, condition (10) which restricts the bias voltage E_0 is too severe; since even if the bias voltage is set as

$$e_2 < E_0 < e_1, \quad (12)$$

in Fig. 4, the circuit in Fig. 2 remains monostable. The condition in (12) is written as

$$2 > a > 1 - \tfrac{2}{3}b,$$

and hence we shall employ the conditions

$$1 > b > 0, \quad c^2 > b, \quad 2 > a > 1 - \tfrac{2}{3}b, \quad (13)$$

instead of (3), for the constants in the BVP model.

V. Propagation of Excitation

The equations which describe the propagation of the excitation along the nerve axon are easily obtained from the equations of the "space clamp."[12]

Denoting the distance along the nerve axon by S (cm), the radius of the nerve axon by R_0 (cm) and the specific resistance of the axoplasm by r_0 (KΩcm), we find that

$$I = \frac{R_0}{2r_0}\frac{\partial^2 V}{\partial S^2}. \quad (14)$$

Consequently, taking (1) into account, the H-H partial differential equations describing the propagation of the excitation become as follows:

$$\begin{cases} \dfrac{\partial^2 V}{\partial S^2} = \dfrac{2r_0}{R_0}\left\{C_0\dfrac{\partial V}{\partial t} + \bar{g}_{Na}m^3h(V - V_{Na}) + \bar{g}_K n^4(V - V_K) + \bar{g}_L(V - V_L)\right\}, \\ \dfrac{\partial m}{\partial t} + \{\alpha_m(V) + \beta_m(V)\}m = \alpha_m(V), \\ \dfrac{\partial h}{\partial t} + \{\alpha_h(V) + \beta_h(V)\}h = \alpha_h(V), \\ \dfrac{\partial n}{\partial t} + \{\alpha_n(V) + \beta_n(V)\}n = \alpha_n(V). \end{cases} \quad (15)$$

Similarly, let us consider the circuit shown in Fig. 5(a) or Fig. 5(b), which is constructed by cascading the many two-terminal circuits of Fig. 2 through interstage coupling resistances.

[11] S. Lefschetz, "Differential Equations: Geometric Theory," Interscience Publishers, New York, N. Y., pp. 249–254; 1957.
[12] Hodgkin and Huxley, *op. cit.*, p. 522.

Regarding the above circuit as a distributed line, we have

$$j = \frac{1}{r}\frac{\partial^2 v}{\partial s^2}, \tag{16}$$

corresponding to (14), provided the interstage coupling resistance per unit length of the line is r. From (2) and (16), it follows that

$$\begin{cases} h\dfrac{\partial^2 u}{\partial s^2} = \dfrac{1}{c}\dfrac{\partial u}{\partial t} - w - \left(u - \dfrac{u^3}{3}\right), \\ c\dfrac{\partial w}{\partial t} + bw = a - u, \end{cases} \tag{17}$$

where $h = \rho/r$.

The system of partial differential equations (17) is the distributed BVP model which may be considered as a simplified system of the H-H partial differential equations (15).

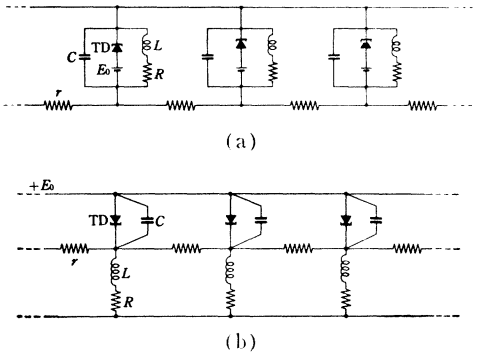

Fig. 5—A distributed active line is obtained by cascading the two-terminal circuits in Fig. 2 through interstage coupling resistances. The circuit shown in (b) is equivalent to that in (a).

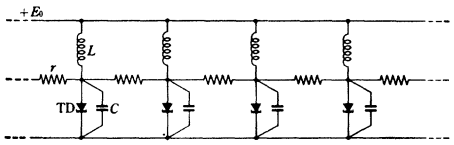

Fig. 6—Electronic model corresponding to (22).

By eliminating w from (17), a single partial differential equation for u is obtained as follows:

$$ch\frac{\partial^3 u}{\partial t \partial s^2} + bh\frac{\partial^2 u}{\partial s^2} = \frac{\partial^2 u}{\partial t^2} - c\left\{\left(1 - \frac{b}{c^2}\right) - u^2\right\}\frac{\partial u}{\partial t} + \left\{(1-b)u + \frac{b}{3}u^3\right\} - a. \tag{18}$$

For simplicity, let us consider a case where $R=0$ $(b=0)$. In such a case, (18) takes the form

$$ch\frac{\partial^3 u}{\partial t \partial s^2} = \frac{\partial^2 u}{\partial t^2} - c(1-u^2)\frac{\partial u}{\partial t} + u - a, \tag{19}$$

where

$$c > 0, \qquad 2 > a > 1, \qquad h > 0. \tag{20}$$

By setting

$$x = \frac{s}{\sqrt{ch}}, \quad z = \frac{2a}{a^2-1}(a-u), \quad \mu = c(a^2-1), \quad \epsilon = \frac{a^2-1}{4a^2}, \tag{21}$$

(19) is transformed as follows:

$$\boxed{\frac{\partial^3 z}{\partial t \partial x^2} = \frac{\partial^2 z}{\partial t^2} + \mu(1 - z + \epsilon z^2)\frac{\partial z}{\partial t} + z, \quad \mu > 0, \quad \frac{3}{16} > \epsilon > 0.} \tag{22}$$

It seems likely that the partial differential equation (22) is one of the simplest mathematical models of the nerve axon. The structure of the electronic model which corresponds to (22) is shown in Fig. 6.

VI. A Boundary-Value Problem

We now proceed to investigate the following boundary-value problem for the partial differential equation (22) (Fig. 7).

$$\begin{cases} z = z(x,t), \ x \geqq 0, \ t \geqq 0, \\ \dfrac{\partial^3 z}{\partial t \partial x^2} = \dfrac{\partial^2 z}{\partial t^2} + \mu(1 - z + \epsilon z^2)\dfrac{\partial z}{\partial t} + z, \\ \mu > 0, \ \dfrac{3}{16} > \epsilon > 0, \\ \text{on the line } t = 0, \ z = 0, \ \dfrac{\partial z}{\partial t} = 0, \\ \text{on the line } x = 0, \ z = F(t)\text{: given.} \end{cases} \tag{23}$$

Some results of the numerical calculation using a digital computer are given below. We chose $\mu = 10$, $\epsilon = 0.1$ and

$$F(t) = \frac{z_0}{2}\left(1 - \cos\frac{2\pi t}{t_0}\right), \qquad t_0 \geqq t \geqq 0, \qquad = 0, \qquad t \geqq t_0. \tag{24}$$

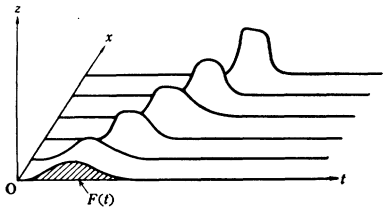

Fig. 7—A schematic display of the boundary-value problem (23).

A. Signal Amplification

The case of $t_0 = 3.0$, $z_0 = 5.0$ is shown in Fig. 8. In this case the signal is amplified in the course of transmission.

B. Signal Attenuation

The case of $t_0 = 1.0$, $z_0 = 20.0$ is shown in Fig. 9. In this case the signal is attenuated in the course of transmission.

C. Signal Elimination

The case of $t_0 = 3.0$, $z_0 = 3.0$ is shown in Fig. 10. In this case the signal is eliminated in the course of transmission.

From these results, it is expected that with respect to the signal height (there being an asymptotic value and a threshold value),

1) a signal with a height between the asymptotic value and the threshold value is amplified during transmission,
2) a signal higher than the asymptotic value is attenuated to the asymptotic value during transmission,
3) a signal lower than the threshold value is eliminated during transmission (see Fig. 11).

These actions may be called "shaping" with respect to signal height. In order to clarify the situation, we shall try to seek for the asymptotic waveform in Section VII.

VII. Asymptotic Waveform

If the partial differential equation (22) has a waveform, as its solution, which is transmitted along a line without suffering distortion and with a constant velocity (say θ), then the solution must be a function of $\tau = t - x/\theta$. In such a case the substitution

$$\xi(\tau) \equiv z(x, t), \qquad \tau = t - \frac{x}{\theta}$$

reduces the partial differential equation (22) to an ordinary differential equation for ξ:

$$\beta\xi''' - \xi'' - \mu(1 - \xi + \epsilon\xi^2)\xi' - \xi = 0, \qquad (25)$$

where $\xi' = d\xi/d\tau$ and

$$\beta = \theta^{-2} > 0. \qquad (26)$$

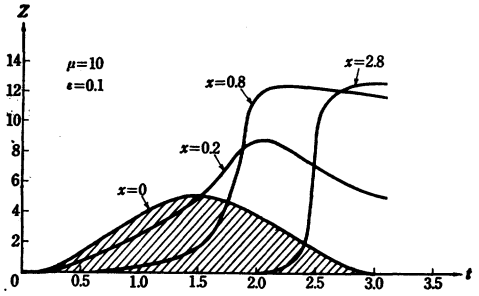

Fig. 8—A signal above the threshold value and below the asymptotic value is amplified during transmission.

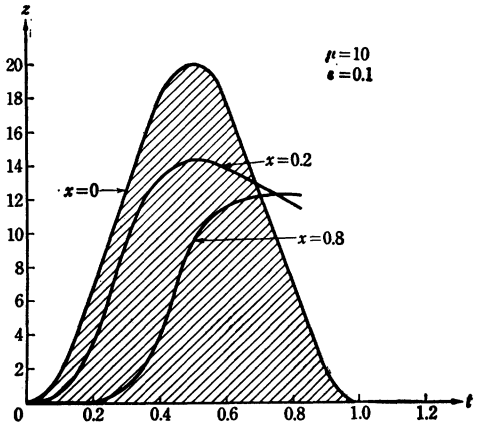

Fig. 9—A signal above the asymptotic value is attenuated during transmission.

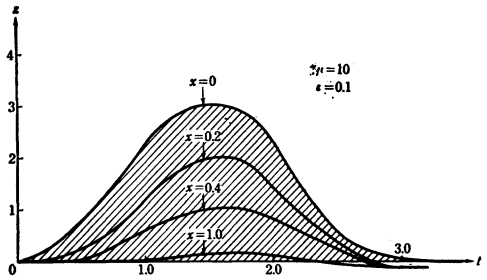

Fig. 10—A signal below the threshold value is eliminated during transmission.

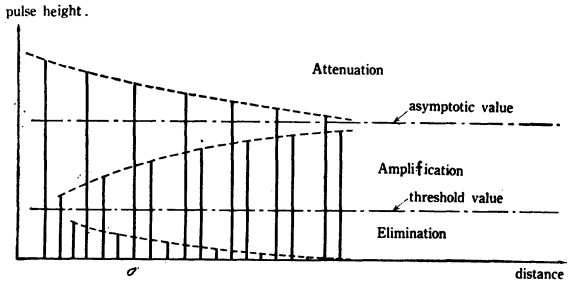

Fig. 11—Signals are amplified or attenuated or eliminated according to their heights.

For the time being, β remains an unknown constant. In fact, its determination constitutes a part of the object of the following procedure. Now, it is obvious that (25) has a resting solution $\xi \equiv 0$. If (25) has a solution, except for $\xi \equiv 0$, such as $\xi(\tau) \to 0$ when $\tau \to \pm \infty$ for some β, then the solution corresponds to the asymptotic waveform which we are seeking, and the transmission velocity of the asymptotic waveform is determined from β.

The behavior of $\xi(\tau)$ in the neighborhood of the resting solution is determined approximately by a linear differential equation

$$\beta\xi''' - \xi'' - \mu\xi' - \xi = 0. \tag{27}$$

The characteristic equation of (27)

$$H(\lambda) \equiv \beta\lambda^3 - \lambda^2 - \mu\lambda - 1 = 0 \tag{28}$$

has one real positive root, since $H(0) = -1 < 0$, $H'(0) = -\mu < 0$ and $H(+\infty) > 0$. By denoting this root as $\lambda_0 (\lambda_0 > 0)$, $H(\lambda)$ is factorized as

$$H(\lambda) = (\lambda - \lambda_0)(\beta\lambda^2 + \gamma\lambda + \lambda_0^{-1}),$$

where

$$\gamma = \beta\lambda_0 - 1 = \frac{\mu}{\lambda_0} + \left(\frac{1}{\lambda_0}\right)^2.$$

Since $\gamma > 0$, it is apparent that both of the other two roots are either real negative or complex conjugate with negative real parts.

From a more precise examination it is easily seen that when $\mu > 2$ and $\beta < \beta_0(\mu)$, they are real negative; otherwise they are complex conjugate with negative real parts, where

$$\beta_0(\mu) = \frac{1}{27}(2\mu^2 - 9\mu + 2\sqrt{\mu^4 - 9\mu^3 + 27\mu^2 - 27}).$$

Now, if $\xi(\tau) \to 0$ when $\tau \to -\infty$, as shown in Fig. 12, then $\xi(\tau) \sim Ae^{\lambda_0\tau}$ (A is an arbitrary constant), when τ has a negative large value. Therefore we have

$$\xi'(\tau) \sim A\lambda_0 e^{\lambda_0\tau}, \qquad \xi''(\tau) \sim A\lambda_0^2 e^{\lambda_0\tau}.$$

We shall perform numerical calculations for the third-order ordinary differential equation (25) with the following initial conditions:

$$\begin{cases} \xi(0) = \Delta, \\ \xi'(0) = \lambda_0\Delta, \\ \xi''(0) = \lambda_0^2\Delta, \end{cases}$$

where $\Delta (\Delta > 0)$ is the smallest step of ξ. It is noted that λ_0 depends on β.

In general, the solution of (25) corresponding to the initial conditions in (29) depends on the value of β; and we are seeking for exactly the β for $\xi(\tau) \to 0$ when $\tau \to +\infty$ as shown in Fig. 12.

When $\mu = 3.0$, $\epsilon = 0.1$, two such values of β were expected to exist from the results of digital computations. One of them is $\beta \doteqdot 0.44488$, which corresponds to a stable asymptotic waveform (Fig. 13), and this is what we are aiming at. The other is $\beta \doteqdot 0.938$ and corresponds to an unstable asymptotic waveform (Fig. 14), which is a critical signal traveling down the line along the threshold and being physically unrealizable.

Because the stable asymptotic waveform is peculiar to this line, it may be expected that the line will show a waveform shaping action, in respect not only to the signal height but also to the signal width.

Fig. 15(a) shows the relation between μ and signal propagation velocity θ in the case of $\epsilon = 0.1$. The velocity of the stable asymptotic waveform seems to be a monotonically increasing function of μ.

Since

$$\frac{\delta s}{\delta t} = \sqrt{ch}\,\theta = \frac{1}{\sqrt{r}}\sqrt[4]{\frac{L}{C}}\,\theta\left(\frac{(e_0 - E_0)^2 - K^2}{\rho K^2}\cdot\sqrt{\frac{L}{C}}\right), \tag{30}$$

the propagation velocity is inversely proportional to $r^{1/2}$. Furthermore, it may be concluded that the velocity increases with increasing L and/or decreasing C, provided $\theta(\mu)$ is monotonically increasing.

Fig. 15(b) shows the relation between μ and pulse height in case of $\epsilon = 0.1$. The shape of the stable asymptotic waveform approaches to a rectangular pulse as μ increases, although its height hardly depends on μ.

It may be expected that the stable asymptotic waveform coincides with the unstable one at $\mu = 2$.

VIII. Experiments

We fabricated a lumped constant cascaded circuit with nine stages as shown in Fig. 16 and the expected results were obtained. In particular, it was observed that the shaping action in respect to the signal height was completed at the first stage, while the shaping action in respect to the signal width was very weak in comparison with the former (Fig. 17).

In order to make the shaping action in respect to pulse height more moderate, it is effective to add some inductance to each interstage coupling resistance in series. The circuit (Fig. 18, page 2068), in the case of $C = 0.05$ μf, shapes traveling signals with respect to the height (Fig. 19). On the other hand, Fig. 20 illustrates the shaping action with respect to the width of the circuit shown in Fig. 18, in the case of $C \doteqdot 20$ pf (junction capacitance of TD).

Since this line has a symmetrical structure, the signal transmission is bidirectional, that is, a signal applied to the right (left) end is transmitted to the left (right) and a signal applied to the middle of the line is transmitted in both directions. An interesting phenomenon is that two signals traveling in opposite direction from both ends vanish at the collision point.

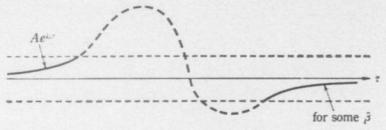

Fig. 12—If (25) has a solution, except for $\xi(\tau)\equiv 0$, such as $\xi(\tau)\to 0$ when $\tau\to+\infty$ for some β, then the solution corresponds to the sought-for asymptotic waveform, and the transmission velocity of the asymptotic waveform is determined from the β.

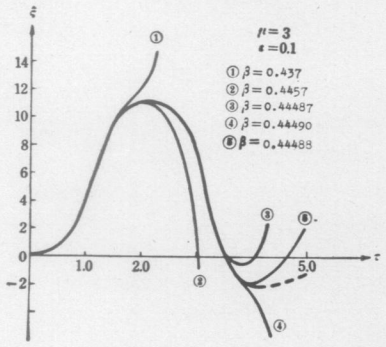

Fig. 13—For $\beta\doteqdot 0.44488$, it is expected that a stable asymptotic waveform exists.

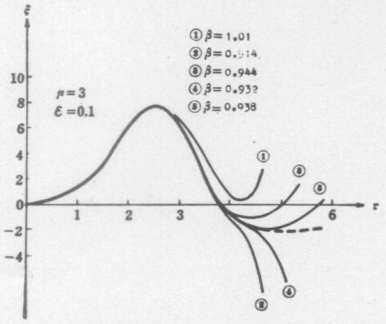

Fig. 14—For $\beta\doteqdot 0.938$, it is expected that an unstable asymptotic waveform exists, which travels down the line along the threshold and is physically unrealizable.

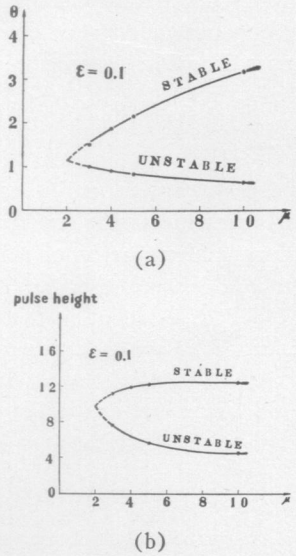

Fig. 15—The relation between μ and the signal propagation velocity and the relation between μ and pulse height in case of $\epsilon=0.1$. It seems that the stable asymptotic waveform coincides with the unstable one at $\mu=2$. (a) The velocity of the stable asymptotic waveform seems to be a monotonically increasing function of μ. (b) The pulse height of the stable asymptotic waveform hardly depends on μ.

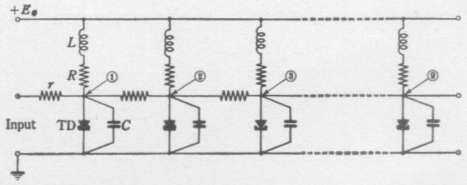

(a)

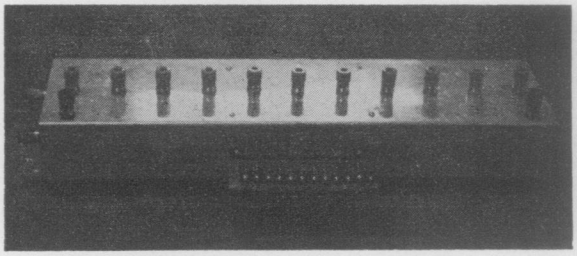

(b)

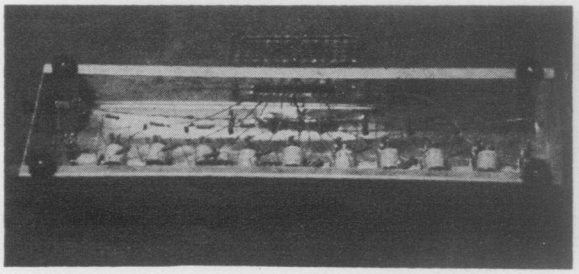

(c)

Fig. 16—The circuit used in our experiments. $L=4$ mh, $R=70\ \Omega$, $r=500\ \Omega$, $E_0=100$ mv, $C=0.01\ \mu$f.

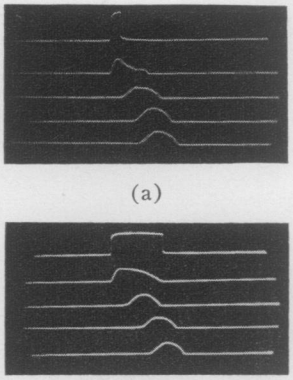

(a)

(b)

Fig. 17—The circuit in Fig. 16 shapes a signal waveform during transmission. In each figure, the first waveform is that of the input signal; the second, third, fourth and the fifth waveforms are those observed at the first, fourth, seventh and the ninth stages in the circuit in Fig. 16(a), respectively. In both cases, the signals achieve the same waveform. (a) A narrow signal (6 μsec) is widened in the course of transmission. (b) A wide signal (32 μsec) is narrowed in the course of transmission.

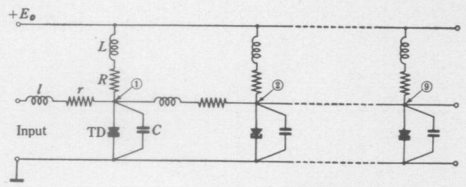

Fig. 18—By adding some inductance to each coupling resistance in series, the shaping action can be made more moderate.

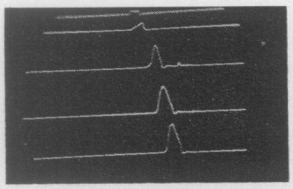

(a)

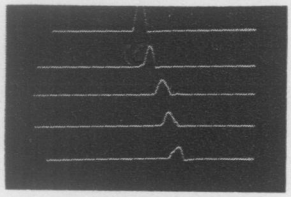

(b)

Fig. 19—Waveform shaping action with respect to the signal height of the circuit in Fig. 18 displayed on a CRO screen. $L=l=4$ mh, $R=115\ \Omega$, $r=200\ \Omega$, $E_0=150$ mv, $C=0.05\ \mu$f. In each figure, the waveform in the first, second, third, fourth and fifth lines are those observed at the first, third, fifth, seventh and ninth stages in the circuit shown in Fig. 18, respectively. Pulse heights in the bottom lines in (a) and (b) are equal and 150 mv. [Note that vertical scales are different in (a) and (b)]. (a) A small signal with 30-mv height is amplified in course of transmission. (b) A large signal with 380-mv height is attenuated in course of transmission.

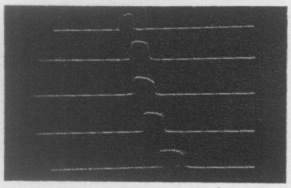

(a)

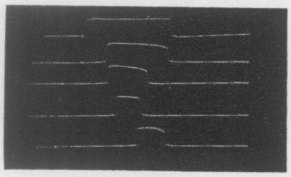

(b)

Fig. 20—Waveform shaping action with respect to the signal width of the circuit in Fig. 18 displayed on a CRO screen. In this case, $C\doteqdot 20$ pf, other constants are the same as those in Fig. 19. The correspondence of lines and stages is the same as that in Fig. 19. Pulse width in the bottom lines of (a) and (b) is equal—10 μsec. (a) A narrow signal with 5-μsec width is widened in the course of transmission. (b) A wide signal with 30-μsec width is narrowed in the course of transmission.

IX. Related Problems

A. The Neuristor

Crane proposed a novel device termed neuristor.[13] A neuristor may be visualized as a one-dimensional channel along which signals may flow. The mode of signal propagation is somewhat analogous to that which occurs along a nerve axon. The neuristor may be used to synthesize all digital logic functions, so that any digital logic system can be realized using arrays of neuristors only. Neuristors are interconnected in two basically different modes—T junctions and S junctions.

Our active pulse transmission line can lead to an electronic realization of the neuristor. The T junction is readily realized by connecting three active pulse transmission lines at a point. The S junction is realized by the circuit in Fig. 21. Corresponding to (22), the differential equations which represent signal propagation along the S junction are as follows:

$$\begin{cases} \dfrac{\partial^3 z_1}{\partial t \partial x^2} = \dfrac{\partial^2 z_1}{\partial t^2} + \mu(1 - z_1 + \epsilon z_1^2)\dfrac{\partial z_1}{\partial t} \\ \qquad\qquad + \dfrac{1}{1-k^2} z_1 + \dfrac{k}{1-k^2} z_2, \\ \dfrac{\partial^3 z_2}{\partial t \partial x^2} = \dfrac{\partial^2 z_2}{\partial t^2} + \mu(1 - z_2 + \epsilon z_2^2)\dfrac{\partial z_2}{\partial t} \\ \qquad\qquad + \dfrac{1}{1-k^2} z_2 + \dfrac{k}{1-k^2} z_1, \end{cases} \tag{31}$$

where $k = M/L$, $0 < k < 1$.

The storage ring of the neuristor was realized by making a loop with forty stages of the monostable circuit and five stages of the S junction (Fig. 22).

Cote has published an active pulse transmission line using *p-n-p-n* diodes toward an electronic realization of the neuristor.[14] The use of current-controlled negative resistance elements, however, seems to make the circuit more complicated.

B. Active Surface

Our active pulse transmission line may easily be extended to an active surface with the structure shown in Fig. 23. The differential equation of this active surface, corresponding to (22), becomes

$$\frac{\partial^3 z}{\partial t \partial x^2} + \frac{\partial^3 z}{\partial t \partial y^2} = \frac{\partial^2 z}{\partial t^2} + \mu(1 - z + \epsilon z^2)\frac{\partial z}{\partial t} + z, \tag{32}$$

$$\mu > 0, \qquad \frac{3}{16} > \epsilon > 0.$$

[13] H. D. Crane, "The neuristor," IRE Trans. on Electronic Computers, vol. EC-9, pp. 370–371, September, 1960; also, "Neuristor Studies," Solid-State Electronics Lab., Stanford University, Stanford, Calif., Tech. Rept. No. 1506-2, July, 1960; also H. D. Crane, "Neuristor—a novel device and system concept," this issue, p. 2048.

[14] A. J. Cote, Jr., "A neuristor prototype," Proc. IRE (*Correspondence*), vol. 49, pp. 1430–1431; September, 1961.

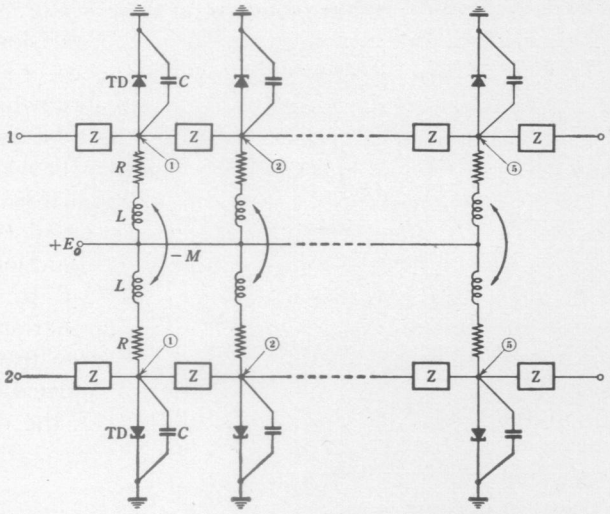

(a)

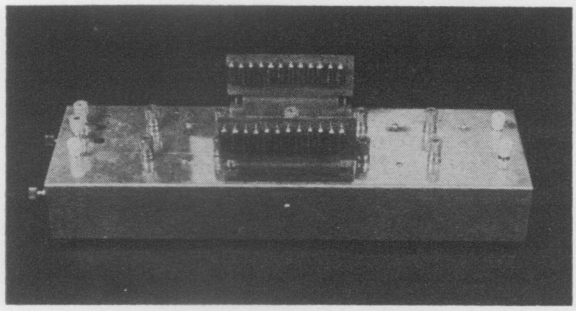

(b)

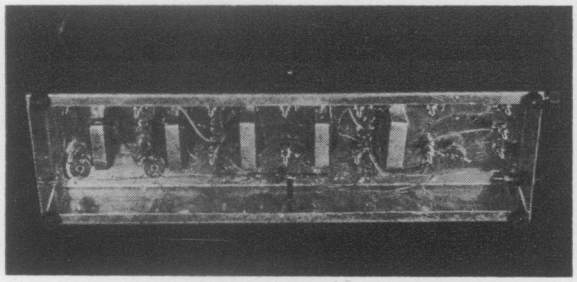

(c)

Fig. 21—An S junction of the neuristor can be realized by coupling two monostable circuits by a mutual inductance. $L=358$ mh, $M=355$ mh, $R=70$ Ω, $Z=r+pl$, $l=4$ mh, $r=70$ Ω, $E_0=70$ mv, $C=0.01$ μf.

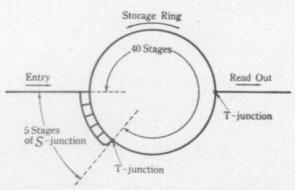

Fig. 22—Signals enter from the "entry" and continue to circulate along the "storage ring." The contents of the storage ring can be obtained from the "read out" line.

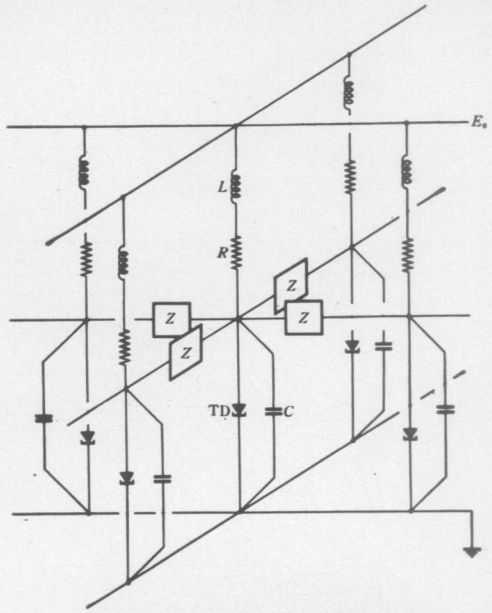

Fig. 23—The structure of the active surface represented by (32).

X. Conclusions

To electronically simulate the distributed BVP model, which may be considered as a simplified Hodgkin-Huxley model describing the propagation of the excitation of the nerve axon, we have made an approximately distributed active pulse transmission line using tunnel diodes. The line behaves similarly to the living axon, but the representation is gross.

The line is constructed by cascading many monostable circuits and consists essentially of the following four parts:

1) transverse power voltage supply,
2) transverse inductance,
3) transverse tunnel diode,
4) longitudinal coupling resistance.

The active line shows the following characteristics in the transmission of signals:

1) There is a certain threshold value in respect to the signal height, and signals below the threshold (or noise) are eliminated during transmission.
2) The line shapes signal waveforms. Namely, there being a specific pulse-like waveform peculiar to this line, signals above the threshold approach it during transmission.
3) Since this line has a symmetrical structure, the signal transmission is bidirectional. Two signals traveling in opposite directions from both ends vanish at the collision point.

On account of the existence of the threshold and the shaping action, this line makes possible highly reliable pulse transmission, and will be useful for various kinds of information-processing systems.

Appendix

We shall briefly sketch the electrical behavior of the surface membrane of a nerve axon following Hodgkin and Huxley.[2]

The electrical behavior of the membrane in the case of a "space clamp" may be represented by the network shown in Fig. 24. Current can be carried through the membrane either by charging the membrane capacity (C_0) or by movement of ions through the resistances in parallel with the capacity.

The capacity current I_C is given by

$$I_C = C_0 \frac{dE}{dt} \cdot \tag{33}$$

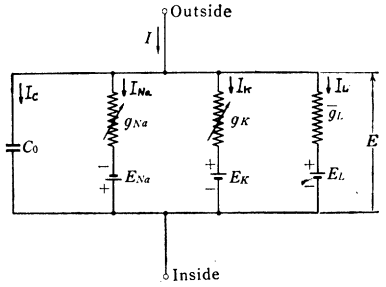

Fig. 24—Equivalent circuit representing the electric behavior of the membrane.

The ionic current is divided into components carried by sodium and potassium ions (I_{Na} and I_K) and a small "leakage current" (I_L) made up by chloride and other ions. Each component of the ionic current is determined by a driving force which may conveniently be measured as an electrical potential difference and a permeability coefficient which has the dimensions of a conductance. Thus the sodium current I_{Na} is equal to the sodium conductance (g_{Na}) multiplied by the difference between the membrane potential E and the equilibrium potential for the sodium ion E_{Na}:

$$I_{Na} = g_{Na}(E - E_{Na}). \tag{34}$$

Similarly we have

$$I_K = g_K(E - E_K), \tag{35}$$

$$I_L = \bar{g}_L(E - E_L). \tag{36}$$

Eqs. (34)–(36) may be rewritten

$$I_{Na} = g_{Na}(V - V_{Na}), \tag{37}$$

$$I_K = g_K(V - V_K), \tag{38}$$

$$I_L = \bar{g}_L(V - V_L), \tag{39}$$

where

$$V = E - E_R, \quad V_{Na} = E_{Na} - E_R, \quad V_K = E_K - E_R,$$

$$V_L = E_L - E_R,$$

and E_R is the absolute value of the resting potential. V, V_{Na}, V_K, and V_L can then be measured directly as displacements from the resting potential.

We then assume that the sodium conductance g_{Na} is represented by

$$g_{Na} = \bar{g}_{Na} m^3 h, \tag{40}$$

$$\frac{dm}{dt} = \alpha_m(1 - m) - \beta_m m, \tag{41}$$

$$\frac{dh}{dt} = \alpha_h(1 - h) - \beta_h h, \tag{42}$$

where $\bar{g}_{Na}$ is a constant with the dimensions of conductance/cm^2; α's and β's are rate constants which vary with voltage (V) but not with time (t) and have dimensions of [time]$^{-1}$; m and h are dimensionless variables which can vary between 0 and 1.

These equations may be given a physical basis if sodium conductance is assumed to be proportional to the number of sites on the inside of the membrane which are occupied simultaneously by three activating molecules but are not blocked by an inactivating molecule. m then represents the proportion of activating molecules on the inside and $1-m$ the proportion on the outside; h is the proportion of inactivating molecules on the outside and $1-h$ the proportion on the inside. α_m or β_h and β_m or α_h represent the transfer rate constants in the two directions.

The forms of α's and β's as functions of V are determined experimentally as shown in (1).

Similar equations for g_K are

$$g_K = \bar{g}_K n^4, \tag{43}$$

$$\frac{dn}{dt} = \alpha_n(1 - n) - \beta_n n. \tag{44}$$

Summing up these equations, we have

$$\begin{aligned} I &= I_C + I_{Na} + I_K + I_L \\ &= C_0 \frac{dV}{dt} + \bar{g}_{Na} m^3 h(V - V_{Na}) + \bar{g}_K n^4 (V - V_K) \\ &\quad + \bar{g}_L(V - V_L), \end{aligned} \tag{45}$$

as shown in (1).

Acknowledgment

The authors appreciate the aid of Dr. S. Nakajima, the aid of Prof. M. Takata and T. Shimizu in the digital computation and the aid of R. Suzuki and Messrs. Saruyama, Takeya and Nozawa in the experiments. The authors also thank Profs. H. Takahashi and S. Furuya for their valuable discussions. This research was supported by a research grant from the Asahi Press, for which we express our deep appreciation.